

1 **Aging of basalt volcanic systems and decreasing CO₂ consumption by weathering**

2 Janine Börker¹, Jens Hartmann¹, Gibran Romero-Mujalli¹, Gaojun Li²

3 ¹Institute for Geology, CEN (Center for Earth System Research and Sustainability), Universität
4 Hamburg, Bundesstraße 55, 20146 Hamburg, Germany. E-Mail: janine.boerker@uni-hamburg.de;
5 geo@hattes.de

6 ²MOE Key Laboratory of Surficial Geochemistry, Department of Earth Sciences, Nanjing
7 University, 163 Xianlindadao, Nanjing 210023, China

8 **Abstract**

9 Basalt weathering is one of many relevant processes balancing the global carbon cycle via land-
10 ocean alkalinity fluxes. The CO₂ consumption by weathering can be calculated using alkalinity
11 and is often scaled with runoff and/or temperature. Here it is tested if the surface age distribution
12 of a volcanic system derived by geological maps is a useful proxy for changes in alkalinity
13 production with time.

14 A linear relationship between temperature normalized alkalinity fluxes and the Holocene area
15 fraction of a volcanic field was identified, using information from 33 basalt volcanic fields, with
16 an $r^2=0.93$. This relationship is interpreted as an aging function and suggests that fluxes from
17 Holocene areas are ~10 times higher than those from old inactive volcanic fields. However, the
18 cause for the decrease with time is probably a combination of effects, including a decrease in
19 alkalinity production from material in the shallow critical zone as well as a decline in hydrothermal
20 activity and magmatic CO₂ contribution. The addition of fresh reactive material on top of the
21 critical zone has an effect in young active volcanic settings which should be accounted for, too.

22 A comparison with global models suggests that global alkalinity fluxes considering Holocene
23 basalt areas are ~60% higher than the average from these models imply. The contribution of
24 Holocene areas to the global basalt alkalinity fluxes is today however only ~5%, because
25 identified, mapped Holocene basalt areas cover only ~1% of the existing basalt areas. The large
26 trap basalt proportion on the global basalt areas today reduces the relevance of the aging effect.
27 However, the aging effect might be a relevant process during periods of globally, intensive
28 volcanic activity, which remains to be tested.

29 **1. Introduction**

30 Basalt areas, despite their limited areal coverage, contribute significantly to CO₂ sequestration by
31 silicate rock weathering (Gaillardet et al., 1999; Dessert et al., 2003; Hartmann et al., 2009). The
32 sensitivity of basalt weathering to climate change (Dessert et al., 2001; Dessert et al., 2003; Coogan
33 and Dosso, 2015; Li et al., 2016) supports a negative weathering feedback in the carbon cycle that

34 maintains the habitability of the Earth's surface over geological time scales (Walker et al., 1981;
35 Berner et al., 1983; Li and Elderfield, 2013). Changes in volcanic weathering fluxes due to
36 emplacement of large volcanic provinces or shifts in the geographic distribution of volcanic fields
37 associated with continental drift may have contributed to climate change in the past (Goddéris et
38 al., 2003; Schaller et al., 2012; Kent and Muttoni, 2013).

39 The role of basalt weathering in the carbon cycle and its feedback strength in the climate system
40 depends, besides the release of geogenic nutrients, on the amount of associated CO₂ consumption
41 and related alkalinity fluxes. The factors that modulate these fluxes are a subject to uncertainty.
42 Previous studies suggest that basalt weathering contributes 25–35% to the global silicate CO₂
43 consumption by weathering (Gaillardet et al., 1999; Dessert et al., 2003; Hartmann et al., 2009).
44 However, their estimations do not consider the potential aging of a weathering system (e.g., Taylor
45 and Blum, 1995). Young volcanic areas can show much higher weathering rates compared to older
46 ones, as was shown for the Lesser Antilles, where a rapid decay of weathering rates within the first
47 0.5 Ma was observed (Rad et al., 2013). Such an aging effect of volcanic areas is difficult to
48 parameterize for global basalt weathering fluxes, due to a lack of global compilations.

49 A practical approach to resolve this issue is to distinguish older and inactive volcanic fields (IVF)
50 and active volcanic fields (AVF) (Li et al., 2016) and compare weathering fluxes with factors
51 driving the weathering process, like land surface temperature or hydrological parameters. By
52 compiling data from 37 basaltic fields globally, Li et al. (2016) showed that spatially explicit
53 alkalinity fluxes (or CO₂ consumption rates) associated with basalt weathering correlate strongly
54 with land surface temperature for IVFs, but not for AVFs. They suggested that previously observed
55 correlations between weathering rates and runoff in global datasets originates partly from the
56 coincidence of high weathering rates and high runoff of AVFs rather than a direct primary runoff
57 control on the weathering rate. Many studied AVFs are located near the oceans and have an
58 elevated topography, a combination, which can cause elevated runoff due to an orographic effect
59 (Gaillardet et al., 2011). However, the effect of aging on weathering rates from a volcanic system
60 discussed here has not been evaluated.

61 The age distribution of the surface area of a whole volcanic system might be used as a first order
62 proxy to study the variability of weathering fluxes of AVFs. However, the exact surface age of
63 volcanic areas is rarely mapped in detail, but Holocene areas are often reported in geological maps.
64 Here, basalt alkalinity fluxes are related to the calculated Holocene areal proportion of volcanic
65 fields at the catchment scale. For this, the concept of weathering reactivity is introduced, which is
66 the relative alkalinity flux of AVFs to the alkalinity flux estimated for IVFs. This reactivity R is
67 compared with the relative age distribution of surface areas, using the proportion of total area
68 occupied by Holocene lavas. From this comparison a function for the decay of alkalinity fluxes
69 with increasing proportion of older land surface area is derived and discussed.

70

71 **2. Methods**

72 The volcanic fields used to establish the relationship between weathering reactivity and Holocene
73 coverage are predominantly described as basalt areas (Li et al., 2016). Based on the availability of
74 detailed geological maps, 33 volcanic provinces were selected, with 19 IVFs and 14 AVFs. A
75 detailed description is given in the Supplementary information. The 14 AVFs are geographically
76 widespread and diverse (Fig.1a). If the absolute age distribution of the volcanic rocks is available,
77 the Holocene areas were mapped using the age range from 11.7 ka to present, according to the
78 International Commission on Stratigraphy version 2017/02 (Cohen et al., 2013). If possible,
79 coordinates of water sample locations were used to constrain catchment boundary to calculate the
80 Holocene fraction for monitored areas. In all cases already existing alkalinity flux calculations
81 were taken from Li et al. (2016). Detailed information on additional mapping and calculations for
82 each system can be found in the Supplementary information (SI).

83 The weathering reactivity (R) of each volcanic field is calculated by normalizing the observed
84 alkalinity flux of the AVF ($F_{\text{calculated}}$, in $10^6 \text{ mol km}^{-2} \text{ a}^{-1}$) to that of the expected flux if the AVF
85 would be an IVF (F_{expected}):

86
$$R = \frac{F_{\text{calculated}}}{F_{\text{expected}}} \quad (\text{eq.1})$$

87

88 where the expected alkalinity flux F_{expected} for IVFs is given by the function (Fig. 1b):

89
$$F_{\text{expected}} (10^6 \text{ mol km}^{-2} \text{ a}^{-1}) = 0.23 * e^{(0.06 * T (^{\circ}C))}, \text{ RMSE} = 0.3 \quad (\text{eq.2})$$

90

91 The root mean square error of the function is represented by RMSE. The parameters of the equation
92 were derived by using a Monte Carlo method, simulating 10,000 runs (for more information see
93 Supplementary information).

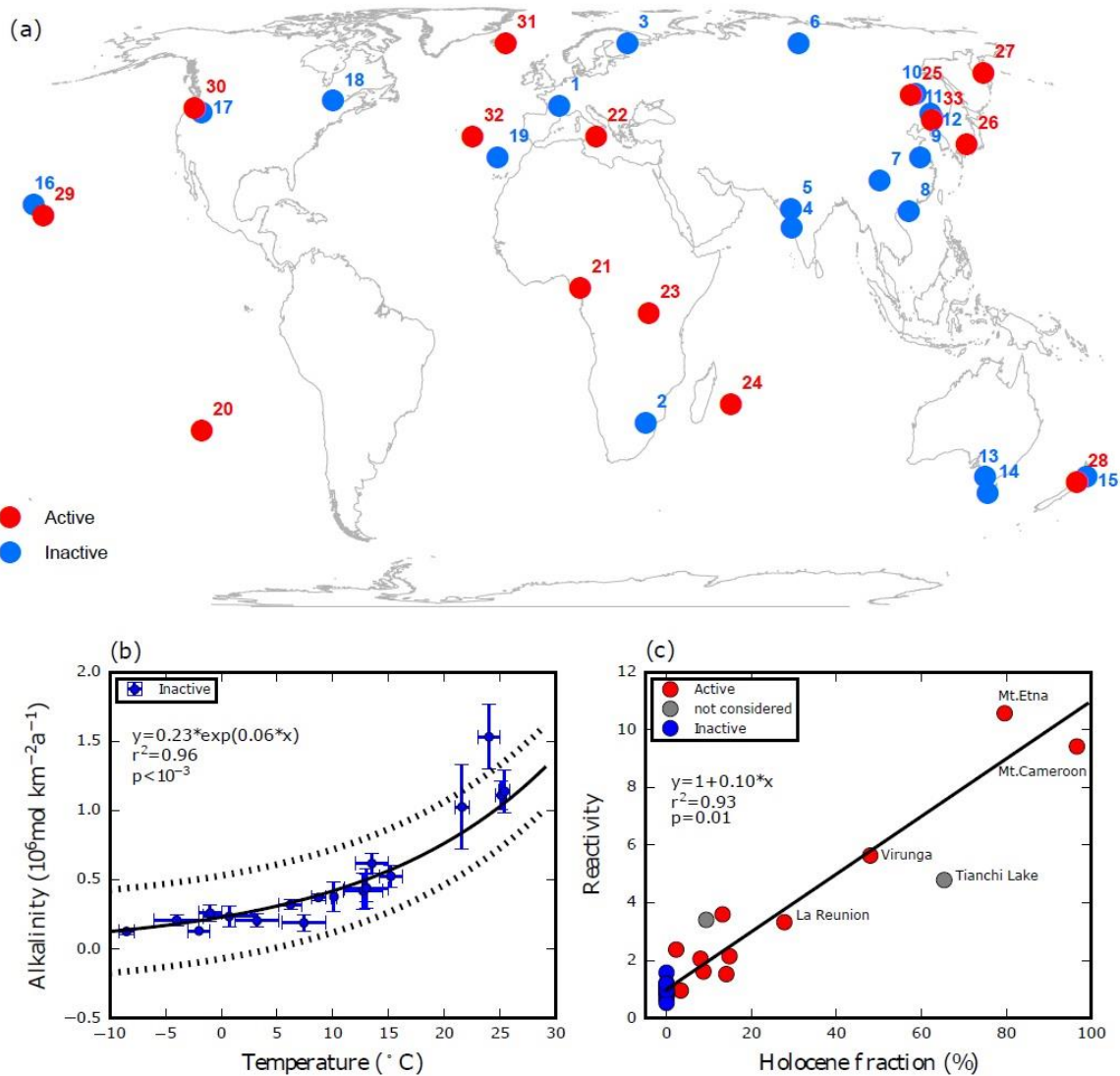


Figure 1(a) The global map shows the locations of the Active Volcanic Fields (in red) and the Inactive Volcanic Fields (in blue) used in this study (1.Massif Central, 2.South Africa, 3.Karelia, 4.Coastal Deccan, 5.Interior Deccan, 6.Siberia Traps, 7.E’Mei, 8.Lei-Qiong, 9.Nanjing, 10.Xiaoxinganling, 11.Tumen River, 12.Mudan River, 13.SE Australia, 14.Tasmania, 15.North Island, NZ, 16.Kauai, Hawaii, 17.Columbia Plateau, 18.NE America, 19.Madeira Island, 20.Easter Island, 21.Mt.Cameroon, 22.Mt.Etna, 23.Virunga, 24.La Réunion, 25.Wudalianchi Lake, 26.Japan, 27.Kamchatka, 28.Taranaki, 29.Big Island, Hawaii, 30.High Cascades, 31.Iceland, 32.Sao Miguel, 33.Tianchi Lake). (b) The exponential relationship between area specific alkalinity flux rates and the land surface temperature for IVFs. The dashed lines represent the range of the mean residual standard deviation of the function (see Supplementary information). Note that r^2 and the p -value were derived by a linear regression of calculated alkalinity flux rates vs. estimated alkalinity flux rates using the new scaling law. (c) The relationship between the Holocene area fraction of the used watersheds from the volcanic fields and the weathering reactivity R . Note that “Tianchi Lake” and “Sao Miguel” are excluded from the calculation of the

regression line because the applied catchments were not dominated by basalt but by trachytic volcanic rock types. Both data points still seem to follow the identified regression trend line for AVFs. R^2 and p -value were calculated by a linear regression of the Holocene fraction vs. reactivity for all AVFs.

94 IVFs group around a reactivity $R=1$ in Fig. 1c, while having a Holocene fraction of zero. The
95 reactivity R (eq. 1) of an AVF can be estimated by the Holocene area fraction as implied by the
96 significant linear correlation identified in Fig. 1c. The theoretical reactivity of a 100% Holocene
97 area H might be estimated by the equation given by Fig. 1c substituting y and x and setting H to
98 100:

99
100
$$R_{100\% \text{ Holocene}} = 1 + 0.10 * H = 11$$
 (eq.3)
101

102 And with this the flux from a young system of only Holocene age:

103
104
$$F_{\text{Holocene}} = R_{100\% \text{ Holocene}} * F_{\text{expected}}$$
 (eq.4)
105

106

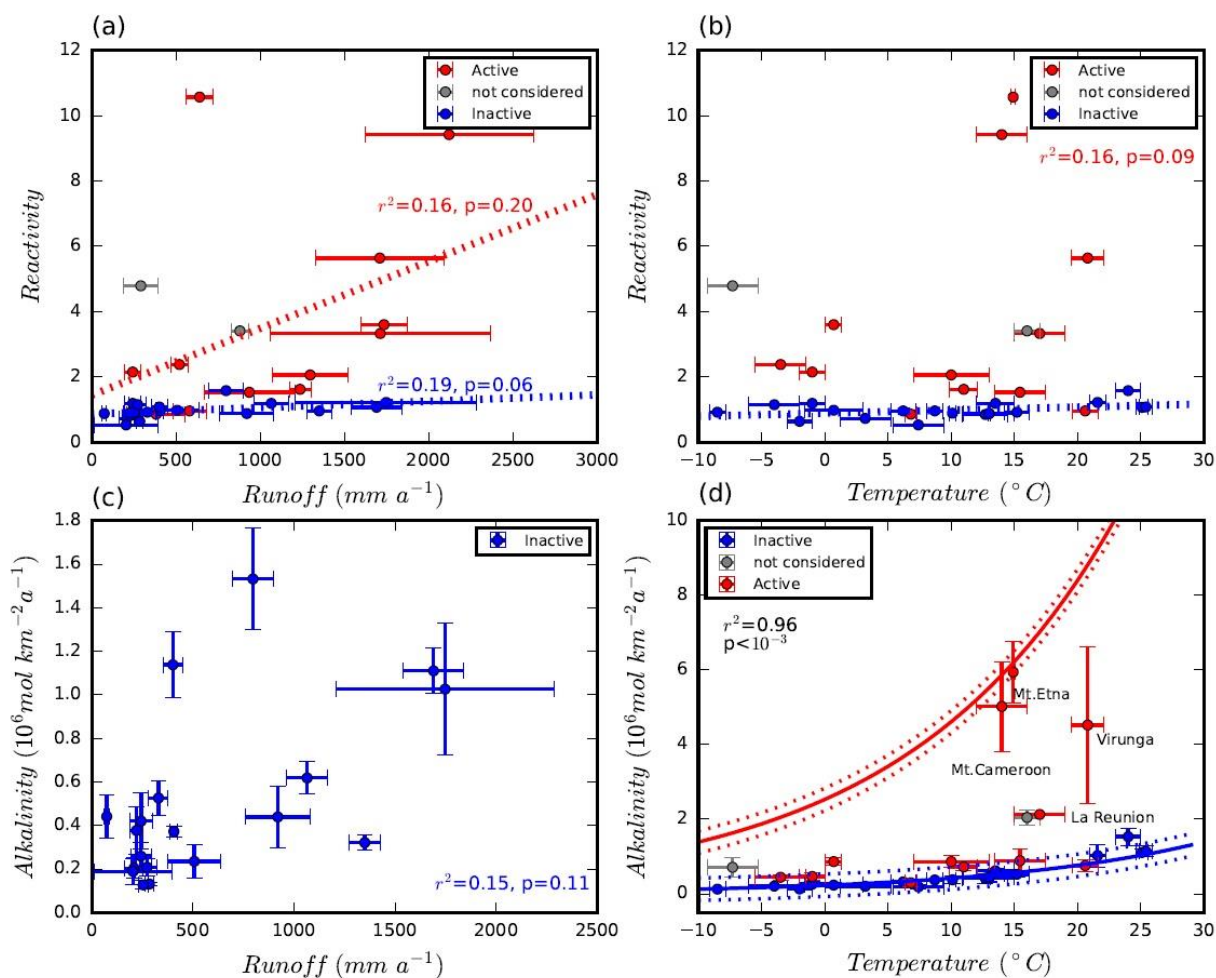


Figure 2(a) shows the runoff-reactivity relationship of all studied volcanic fields. The blue regression line (IVFs) suggests almost no correlation of reactivity with runoff, also for the AFVs no significant correlation is identified (coefficient of determination $r^2=0.16$ ($p=0.20$)) (b) Reactivity versus temperature suggests no bias of reactivity due to a temperature effect for AVFs, as reactivity is based on a temperature normalized parameterization. For the IVFs ($r^2=0.16$, $p=0.09$) no bias with temperature can be identified due to the good correlation of alkalinity fluxes with land surface temperature (blue line) (c) Runoff versus alkalinity flux rates for inactive volcanic fields shows no significant correlation ($r^2=0.15$, $p=0.11$) (d) Temperature versus alkalinity flux rates for all volcanic fields of the study. The blue line represents the new scaling law for IVFs and the red line the new scaling law for AVFs with 100% Holocene area coverage (calculated deviation is represented by dashed lines). R^2 and p -value are derived by a linear regression of calculated alkalinity flux rates vs. observed alkalinity flux rates for all volcanic fields.

110 Global alkalinity fluxes from basalt areas were calculated by using equation 2 for older areas than
111 of Holocene age and equation 4 for mapped Holocene areas. These equations (eq.2 and following,
112 using information based on eq.2) were calibrated for areas with a runoff $> 74 \text{ mm a}^{-1}$ (the lowest
113 runoff value in data compilation of Li et al. (2016) and therefore limit of the model setup) to avoid
114 too high alkalinity fluxes from drier areas with high temperature (*e.g.*, the Sahara Desert),
115 assuming that neglecting fluxes from areas with lower runoff are not biasing the comparison (Tab.
116 S1, Supplementary information). In this case an overestimation is avoided. For the global
117 calculation of CO_2 consumption by the new scaling law, a Monte Carlo method simulating 10,000
118 runs was applied (see Supplementary information).

119 Results are compared with four previous global empirical alkalinity flux models (Bluth and Kump,
120 1994; Amiotte-Suchet and Probst, 1995; Dessert et al., 2003; Goll et al., 2014). Alkalinity fluxes
121 were translated into CO_2 consumption to allow for comparison with previous literature. For all
122 models the same data input was used: a newly compiled global basalt map (mostly derived by the
123 basalt lithological layer from the GLiM, but enhanced by mapped Holocene areas (Supplementary
124 information; Hartmann and Moosdorf, 2012), additional regional geological maps describing
125 basalt areas and the maps of the volcanic fields used in this study, for detailed information see
126 Supplementary information), temperature (Hijmans et al., 2005) and runoff (Fekete et al., 2002).

127

128 **3. Results and Discussion**

129 Studied IVFs are characterized by a Holocene volcanic surface area of 0% with weathering
130 reactivity R ranging between 0.5 and 1.6 (Fig. 1c). In contrast, AVFs show a large range of
131 Holocene coverage, from 0.2% (High Cascades) to 96.6% (Mount Cameroon), and weathering
132 reactivity between 0.9 (High Cascades) and 10.6 (Mount Etna). The weathering reactivity
133 correlates strongly with the percentage of Holocene area ($r^2 = 0.93$; Fig. 1c), suggesting Holocene
134 surface area distribution to be a good predictor for the enhanced alkalinity fluxes from a volcanic
135 system:

$$136 \quad F_{alkalinity} = (1 + 0.10 * H) * 0.23 * e^{(0.06 * T)} [10^6 \text{ mol km}^{-2} \text{ a}^{-1}], \text{ RMSE} = 0.3 \quad (\text{eq.5})$$

137 where H is the Holocene fraction of a volcanic system in % and T is land surface temperature in
138 $^{\circ}\text{C}$.

139 The Holocene fraction is not interpreted as the physical cause for elevated alkalinity fluxes.
140 Instead, magmatic CO_2 contribution, geothermal-hydrothermal activity and the input of new
141 volcanic material on top of the surface (properties and “freshness” of the surface area for reaction)
142 are contributing to enhanced alkalinity fluxes. Volcanic ashes and ejecta might contribute to
143 elevated weathering fluxes because of a relatively high content of glass. Glass dissolution rates are
144 relatively high compared to mineral dissolution rates in general, but base cation content release
145 varies dependent on the Si:O ratio (Wolff-Boenisch et al., 2006).

146 The magmatic CO₂ contributions to alkalinity fluxes in young volcanic systems may be large in
147 general, but data are scarce to evaluate the global relevance for AVFs. For the Lesser Antilles a
148 magmatic contribution of 23 to 40% to the CO₂ consumed by weathering was identified (Rivé et
149 al., 2013). High ¹³C-DIC values suggest that magmatic CO₂ contributes significantly to the
150 alkalinity fluxes from the Virunga system (Balagizi et al., 2015). The magmatic CO₂ contribution
151 derived from volcanic calcite dissolution on Iceland was estimated to be about 10% of the
152 alkalinity fluxes for the studied area (Jacobson et al., 2015). In case of the Etna 7% of the CO₂
153 emitted due to volcanic activity may be captured by weathering (Aiuppa et al., 2000). These
154 examples suggest that significant amounts of magmatic carbon may be transferred to the ocean
155 directly via intra-volcanic weathering from AVFs.

156 These examples show that in case of active volcanic fields the traditional view on kinetic versus
157 supply limitation in the “shallow” critical zone in context of tectonic settings does not hold (e.g.,
158 Ferrier et al., 2016). In contrary the supply of fresh material on top of the classical critical zone
159 and the weathering from below the classical critical zone, suggests that these hot spots of silicate
160 weathering in active volcanic areas, which contribute over proportionally to the global CO₂
161 consumption by silicate weathering, demand likely a different way of looking at it. The blue data
162 points (IVF) in Figure 2d suggest a kinetic limited regime and follow a temperature dependency.
163 The red points (AVF) however are located above the data points of IVF in general. Taking into
164 account that the four AVFs Mt. Etna, Mt. Cameroon, Virunga and La Reunion have the highest
165 Holocene fractions (96.6%-27.7%) and that the further AVFs, which have less than 15% Holocene
166 coverage are located in general above the regression line for IVFs, supports the argument that a
167 combination of elevated geothermal fluxes, magmatic CO₂ and fresh material supplied on top of
168 the classical critical zone contribute to the observed elevated alkalinity fluxes for AVFs in general.

169 The calculated global basalt weathering alkalinity fluxes based on previous global models (Bluth
170 and Kump, 1994; Amiotte-Suchet and Probst, 1995; Dessert et al., 2003; Goll et al., 2014) give
171 alkalinity fluxes ranging between 0.8 to 1.7 ×10¹² mol a⁻¹. These values are different to previously
172 published results based on the same models because a different geological map and climate data
173 are used in this study. The new scaling law calculation based on the temperature dependence of
174 weathering rate and the age dependence of weathering reactivity (eq. 4) results in higher global
175 alkalinity fluxes of 1.9×10¹² mol a⁻¹ and 3.3 ×10¹² mol a⁻¹ for regions with > 74mm a⁻¹ runoff, and
176 for all areas, respectively. The latter higher estimate is mainly due to the modeled contribution
177 from dry and hot regions and shows that it is relevant to apply the runoff cut off.

178 Using the introduced new approach, considering the aging of a volcanic system, reveals that
179 alkalinity fluxes from Holocene areas contribute today only 5% to the global basalt weathering
180 alkalinity flux. This is because so far identified mapped Holocene volcanic areas cover only ~1%
181 of all basalt areas. This study did not include areas of less mafic volcanic areas, like andesites, or
182 middle American volcanics.

183 The Holocene area is probably underestimated due to information gaps in the reported age
 184 information of the global map. The strong dependence of weathering reactivity on relative age of
 185 the surface of a considered volcanic system suggests that it is relevant to know the global spatial
 186 age distribution of volcanic areas in more detail. Therefore, a new global review of the age
 187 distribution of basalt areas would be needed, which is beyond the scope of this study. The
 188 lithologies, predominantly described as basaltic in the global map, might introduce an additional
 189 bias to the global calculations because heterogeneities in the lithology cannot be excluded. Two
 190 active volcanic fields (Sao Miguel and Tianchi Lake) were excluded from the calculation of the
 191 scaling law function because available catchments with alkalinity data hold largely lithologies of
 192 trachytic composition. Nevertheless, their data points (Fig. 1c) seem to show the same weathering
 193 behavior.

194

Table 1: Summary of global basalt CO₂ consumption rates for different models and the new parameterization. For simplicity it was assumed that alkalinity fluxes equal CO₂ consumption. The percentiles of the values of the global calculation by the new scaling law (Monte Carlo method) can be found in the Supplementary information. The standard deviation is given below as described in the Supplementary information.

Models for comparison	parameters	Global CO ₂ consumption rate (10 ⁹ mol/a) for limited area in comparison (only areas with > 74mm/a runoff)	Global CO ₂ consumption rate (10 ⁹ mol/a)
Dessert et al. 2003	runoff, temperature	1669	1684
Amiotte-Suchet & Probst, 1995	runoff	863	870
Bluth & Kump, 1994	runoff	746	761
Goll et al., 2014	runoff, temperature	1566	1580
New scaling law	temperature	1930 ± 90	3300 ± 200

195

196 The applied time period of the Holocene boundary suggests that the aging of the “weathering
 197 motor” of a basaltic volcanic area, including internal weathering, with declining volcanic activity
 198 is rather rapid. This implies that peaks in global volcanic activity have probably a short but
 199 intensive effect on the CO₂ consumption. A pronounced effect on the global carbon cycle by
 200 shifting the global reactivity of volcanic areas may only be relevant for geological periods with
 201 significantly elevated production of new volcanic areas, accompanied by geothermal-
 202 hydrothermal activity and capture of magmatic CO₂ before its escape to the atmosphere.

203 Results may have relevance for the carbon cycle and climate studies exploring the emplacement
 204 of large igneous provinces like the CAMP (Schaller et al., 2012) or the Deccan traps (Caldeira and
 205 Rampino, 1990) with production of large basaltic areas within a short time. However, the

206 biological contribution to CO₂ drawdown, via elevated fertilization effects, *e.g.* P- or Si-release
207 due to weathering and elevated CO₂ in the atmosphere should be taken into account, too.

208 Looking deeper into Earth's history: variations in the solid Earth CO₂ degassing rate or changes in
209 environmental conditions affecting the weathering intensity (Teitler et al., 2014; Hartmann et al.,
210 2017) may have caused different reactivity patterns in dependence of surface age as shown here.

211 In conclusion, a simple approach to detect an aging effect, using surface age as a proxy for several
212 combined processes, was chosen due to availability of data. It can be shown that there exists a
213 linear relationship between temperature normalized alkalinity fluxes and the Holocene area
214 fraction of a volcanic system. Nevertheless, the combined effect on elevated weathering reactivity
215 due to magmatic CO₂ contribution, hydrothermal activity, production of fresh surface area for
216 reaction, and hydrological factors of young volcanic systems remains to be disentangled, for single
217 volcanic systems, as well as for the emplacement of larger, trap-style basalt areas.

218

219 **Acknowledgements:**

220 Funding for this work has been provided by German Research Foundation (DFG) through the
221 Cluster of Excellence CLISAP2 (DFG Exec177, Universität Hamburg) and BMBF-project
222 PALMOD (Ref 01LP1506C) through the German Federal Ministry of Education and Research
223 (BMBF) as Research for Sustainability initiative (FONA). G.L. is supported by National Natural
224 Science Foundation of China (grants 41761144058 and 41730101). The authors thank the editor,
225 R. Emberson and one anonymous reviewer for constructive comments on the manuscript.

226 **6. References**

- 227 Aiuppa, A., Allard, P., D'Alessandro, W., Michel, A., Parello, F., Treuil, M., and Valenza, M.: Mobility and
228 fluxes of major, minor and trace metals during basalt weathering and groundwater transport at Mt. Etna
229 volcano (Sicily), *Geochimica et Cosmochimica Acta*, 64, 1827-1841, 2000.
- 230 Amiotte-Suchet, P., and Probst, J. L.: A global model for present-day atmospheric/soil CO₂ consumption
231 by chemical erosion of continental rocks (GEM-CO₂), *Tellus B*, 47, 273-280, 10.1034/j.1600-
232 0889.47.issue1.23.x, 1995.
- 233 Balagizi, C. M., Darchambeau, F., Bouillon, S., Yalire, M. M., Lambert, T., and Borges, A. V.: River
234 geochemistry, chemical weathering, and atmospheric CO₂ consumption rates in the Virunga Volcanic
235 Province (East Africa), *Geochemistry, Geophysics, Geosystems*, 16, 2637-2660, 10.1002/2015GC005999,
236 2015.
- 237 Berner, R. A., Lasaga, A. C., and Garrels, R. M.: The carbonate-silicate geochemical cycle and its effect on
238 atmospheric carbon dioxide over the past 100 million years, *Am J Sci*, 283, 641-683, 1983.
- 239 Bluth, G. J., and Kump, L. R.: Lithologic and climatologic controls of river chemistry, *Geochimica et*
240 *Cosmochimica Acta*, 58, 2341-2359, 1994.
- 241 Caldeira, K., and Rampino, M. R.: Carbon dioxide emissions from Deccan volcanism and a K/T boundary
242 greenhouse effect, *Geophysical Research Letters*, 17, 1299-1302, 1990.
- 243 Cohen, K., Finney, S., Gibbard, P., and Fan, J.-X.: The ICS international chronostratigraphic chart,
244 *Episodes*, 36, 199-204, 2013.

245 Coogan, L. A., and Dosso, S. E.: Alteration of ocean crust provides a strong temperature dependent
246 feedback on the geological carbon cycle and is a primary driver of the Sr-isotopic composition of
247 seawater, *Earth and Planetary Science Letters*, 415, 38-46, <http://dx.doi.org/10.1016/j.epsl.2015.01.027>,
248 2015.

249 Dessert, C., Dupré, B., François, L. M., Schott, J., Gaillardet, J., Chakrapani, G., and Bajpai, S.: Erosion of
250 Deccan Traps determined by river geochemistry: impact on the global climate and the $^{87}\text{Sr}/^{86}\text{Sr}$ ratio of
251 seawater, *Earth and Planetary Science Letters*, 188, 459-474, [http://dx.doi.org/10.1016/S0012-
252 821X\(01\)00317-X](http://dx.doi.org/10.1016/S0012-821X(01)00317-X), 2001.

253 Dessert, C., Dupré, B., Gaillardet, J., François, L. M., and Allègre, C. J.: Basalt weathering laws and the
254 impact of basalt weathering on the global carbon cycle, *Chemical Geology*, 202, 257-273,
255 <http://dx.doi.org/10.1016/j.chemgeo.2002.10.001>, 2003.

256 Fekete, B. M., Vörösmarty, C. J., and Grabs, W.: High - resolution fields of global runoff combining
257 observed river discharge and simulated water balances, *Global Biogeochemical Cycles*, 16, 2002.

258 Ferrier, K. L., Riebe, C. S., and Jesse Hahm, W.: Testing for supply - limited and kinetic - limited chemical
259 erosion in field measurements of regolith production and chemical depletion, *Geochemistry,
260 Geophysics, Geosystems*, 17, 2270-2285, 2016.

261 Gaillardet, J., Dupré, B., Louvat, P., and Allègre, C. J.: Global silicate weathering and CO_2 consumption
262 rates deduced from the chemistry of large rivers, *Chemical Geology*, 159, 3-30,
263 [http://dx.doi.org/10.1016/S0009-2541\(99\)00031-5](http://dx.doi.org/10.1016/S0009-2541(99)00031-5), 1999.

264 Gaillardet, J., Rad, S., Rivé, K., Louvat, P., Gorge, C., Allègre, C. J., and Lajeunesse, E.: Orography-driven
265 chemical denudation in the Lesser Antilles: Evidence for a new feed-back mechanism stabilizing
266 atmospheric CO_2 , *American journal of science*, 311, 851-894, 2011.

267 Goddérís, Y., Donnadieu, Y., Nédélec, A., Dupré, B., Dessert, C., Grard, A., Ramstein, G., and François, L.
268 M.: The Sturtian 'snowball' glaciation: fire and ice, *Earth and Planetary Science Letters*, 211, 1-12,
269 [http://dx.doi.org/10.1016/S0012-821X\(03\)00197-3](http://dx.doi.org/10.1016/S0012-821X(03)00197-3), 2003.

270 Goll, D. S., Moosdorf, N., Hartmann, J., and Brovkin, V.: Climate-driven changes in chemical weathering
271 and associated phosphorus release since 1850: Implications for the land carbon balance, *Geophysical
272 Research Letters*, 41, 3553-3558, 10.1002/2014GL059471, 2014.

273 Hartmann, J., Jansen, N., Dürr, H. H., Kempe, S., and Köhler, P.: Global CO_2 -consumption by chemical
274 weathering: What is the contribution of highly active weathering regions?, *Global and Planetary Change*,
275 69, 185-194, 2009.

276 Hartmann, J., and Moosdorf, N.: The new global lithological map database GLiM: A representation of
277 rock properties at the Earth surface, *Geochemistry, Geophysics, Geosystems*, 13, n/a-n/a,
278 10.1029/2012gc004370, 2012.

279 Hartmann, J., Li, G., and West, A. J.: Running out of gas: Zircon ^{18}O -Hf-U/Pb evidence for Snowball Earth
280 preconditioned by low degassing, *Geochemical Perspectives Letters*, 4, 41-46,
281 <http://dx.doi.org/10.7185/geochemlet.1734>, 2017.

282 Hijmans, R. J., Cameron, S. E., Parra, J. L., Jones, P. G., and Jarvis, A.: Very high resolution interpolated
283 climate surfaces for global land areas, *International journal of climatology*, 25, 1965-1978, 2005.

284 Jacobson, A. D., Grace Andrews, M., Lehn, G. O., and Holmden, C.: Silicate versus carbonate weathering
285 in Iceland: New insights from Ca isotopes, *Earth and Planetary Science Letters*, 416, 132-142,
286 <http://dx.doi.org/10.1016/j.epsl.2015.01.030>, 2015.

287 Kent, D. V., and Muttoni, G.: Modulation of Late Cretaceous and Cenozoic climate by variable drawdown
288 of atmospheric pCO_2 from weathering of basaltic provinces on continents drifting through the
289 equatorial humid belt, *Clim. Past*, 9, 525-546, 10.5194/cp-9-525-2013, 2013.

290 Li, G., and Elderfield, H.: Evolution of carbon cycle over the past 100 million years, *Geochimica et
291 Cosmochimica Acta*, 103, 11-25, <http://dx.doi.org/10.1016/j.gca.2012.10.014>, 2013.

292 Li, G., Hartmann, J., Derry, L. A., West, A. J., You, C.-F., Long, X., Zhan, T., Li, L., Li, G., Qiu, W., Li, T., Liu,
293 L., Chen, Y., Ji, J., Zhao, L., and Chen, J.: Temperature dependence of basalt weathering, *Earth and*
294 *Planetary Science Letters*, 443, 59-69, <http://dx.doi.org/10.1016/j.epsl.2016.03.015>, 2016.
295 Rad, S., Rivé, K., Vittecoq, B., Cerdan, O., and Allègre, C. J.: Chemical weathering and erosion rates in the
296 Lesser Antilles: An overview in Guadeloupe, Martinique and Dominica, *Journal of South American Earth*
297 *Sciences*, 45, 331-344, <http://dx.doi.org/10.1016/j.jsames.2013.03.004>, 2013.
298 Rivé, K., Gaillardet, J., Agrinier, P., and Rad, S.: Carbon isotopes in the rivers from the Lesser Antilles:
299 origin of the carbonic acid consumed by weathering reactions in the Lesser Antilles, *Earth Surface*
300 *Processes and Landforms*, 38, 1020-1035, 10.1002/esp.3385, 2013.
301 Schaller, M. F., Wright, J. D., Kent, D. V., and Olsen, P. E.: Rapid emplacement of the Central Atlantic
302 Magmatic Province as a net sink for CO₂, *Earth and Planetary Science Letters*, 323–324, 27-39,
303 <http://dx.doi.org/10.1016/j.epsl.2011.12.028>, 2012.
304 Taylor, A., and Blum, J. D.: Relation between soil age and silicate weathering rates determined from the
305 chemical evolution of a glacial chronosequence, *Geology*, 23, 979-982, 1995.
306 Teitler, Y., Le Hir, G., Fluteau, F., Philippot, P., and Donnadieu, Y.: Investigating the Paleoproterozoic
307 glaciations with 3-D climate modeling, *Earth and Planetary Science Letters*, 395, 71-80,
308 <http://dx.doi.org/10.1016/j.epsl.2014.03.044>, 2014.
309 Walker, J. C. G., Hays, P. B., and Kasting, J. F.: A negative feedback mechanism for the long-term
310 stabilization of Earth's surface temperature, *Journal of Geophysical Research: Oceans*, 86, 9776-9782,
311 10.1029/JC086iC10p09776, 1981.
312 Wolff-Boenisch, D., Gislason, S. R., and Oelkers, E. H.: The effect of crystallinity on dissolution rates and
313 CO₂ consumption capacity of silicates, *Geochimica et Cosmochimica Acta*, 70, 858-870, 2006.

314